

## ABLATIVE HELE–SHAW MODEL FOR ICF FLOWS MODELING AND NUMERICAL SIMULATION

HUGUES EGLY

*Michelin, Clermont-ferrand, France*

BRUNO DESPRÉS

*Laboratoire J. L. Lions, Paris, France  
despres@ann.jussieu.fr*

REMI SENTIS

*CEA/DIF, 91297 Arpajon Cedex, France*

Received 23 February 2010

Revised 14 October 2010

Communicated by A. Vasseur

We propose a model for the study of ablation fronts encountered in inertial confinement fusion flows. Following the ideas of physicists specially Sanz's ones, we try to justify the modeling of this problem by a Hele–Shaw equation posed in the complement of a bounded domain the boundary of which is evolving with time. This equation is coupled with an advection equation for the vorticity of the fluid. We propose a numerical strategy based on the fat boundary method to discretize the system and we present some numerical results which show that the numerical method is feasible to simulate ablative Raleigh–Taylor instabilities in the context of these plasma flows.

AMS Subject Classification: 22E46, 53C35, 57S20

### 1. Introduction

In the framework of inertial confinement fusion (ICF) experiments, one problem concerns the implosion of a capsule containing the deuterium tritium fuel, see Fig. 1. A spherical shell which is initially cold is heated by a very intense thermal flux and therefore a plasma is accelerated toward the center of the target.<sup>19</sup> As a matter of fact, there is a first shock and a reflective shock which travel through the capsule, thus all the matter is driven with a macroscopic radial velocity  $\mathbf{u}_{\text{macro}}$ . For modeling this complex flow, it is natural to perform a change of the reference frame corresponding to this macroscopic velocity. Since the velocity  $\mathbf{u}_{\text{macro}}$  depends on time, an

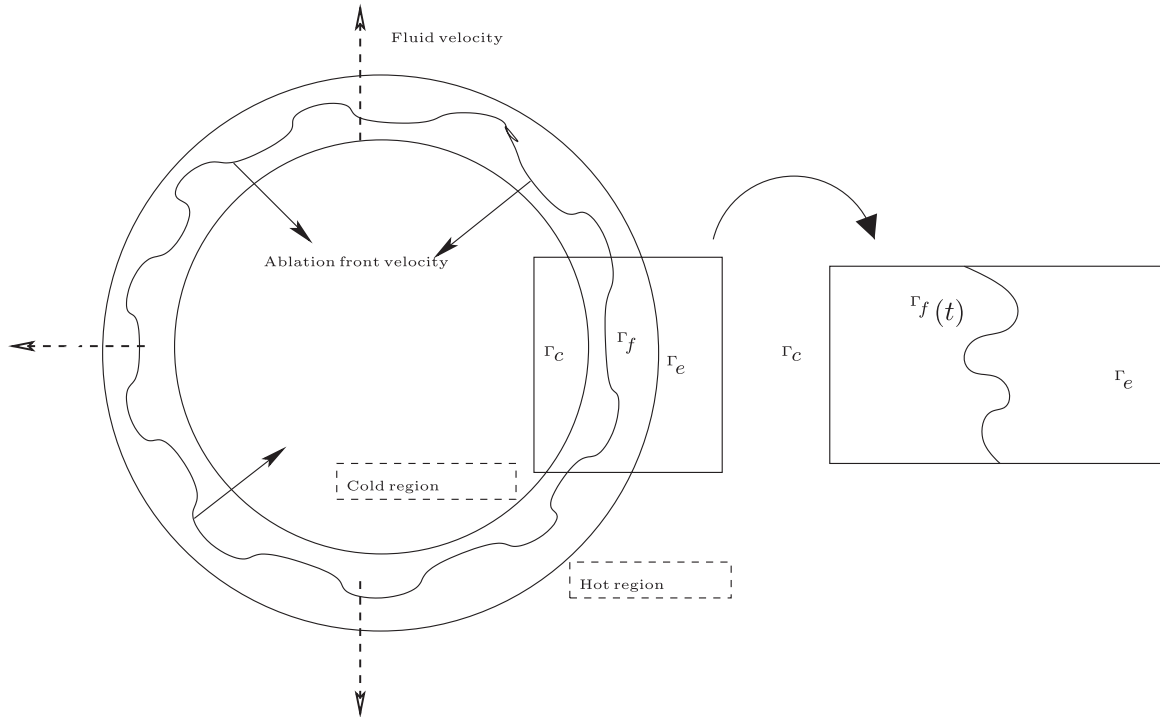


Fig. 1. Inertial confinement fusion convergent geometry. A heat flux comes from the external boundary  $\Gamma_e$ , so that an ablation front  $\Gamma_f$  propagates toward the center of the shell. The front  $\Gamma_f$  may be considered as a moving frontier. Notice the equivalence with Cartesian geometry.

acceleration force denoted in what follows by  $\mathbf{g}$  is exerted on the shell. Moreover the shell is highly heated and it is crucial to account for thermal conduction. Lastly, the material velocity (in the moving reference frame) is small if compared to the speed of sound, then the flow is a quasi-isobar one and we can model it by performing a classical low Mach number approximation; that is, if  $T$  and  $\rho$  denote the temperature and the density, we may assume that the pressure  $\rho T$  is approximatively constant. After performing a good scaling, one may address the following quasi-isobar Euler system with  $\rho T = 1$ :

$$\begin{cases} \partial_t \rho + \nabla \cdot (\rho \mathbf{u}) = 0, \\ \rho(\partial_t + \mathbf{u} \cdot \nabla) \mathbf{u} + \nabla P = \rho \mathbf{g}, \\ \nabla \cdot (\mathbf{u} - n T^n \nabla T) = 0. \end{cases} \quad (1.1)$$

Here  $P$  is the variation of pressure,  $\mathbf{u}$  the velocity and the thermal conduction flux is denoted by  $-n T^n \nabla T$  with  $n$  such that  $\frac{3}{2} \leq n \leq \frac{7}{2}$  (depending on the physical conditions). We refer to the Appendix for a justification of this model. In the case  $n = 0$  this system is a classical incompressible Euler model with variable density.<sup>20</sup> In the case  $n > 0$  which is our concern, it may be called a quasi-incompressible model.

From a physical point of view the shell is highly heated. Therefore a surface is dynamically created where the temperature gradient is very sharp; by the way there is also a very sharp gradient (in the opposite direction) of the density near this surface. This phenomenon is called an *ablation front*. We refer to Ref. 19 for a

comprehensive physical presentation of the topic: a schematic ablation front is described in the zoom in Fig. 1 and also in the Appendix. Actually the numerical treatment of ablation fronts is the source of some major difficulties. Due to the acceleration which is equivalent to a gravity term, the instability of the surface is of Rayleigh–Taylor type: it has been observed that the growth of the so-called *ablation Rayleigh–Taylor* instability depends strongly on the thermal conduction phenomenon<sup>28</sup> (see also Refs. 21 and 27 for theoretical and numerical studies related to the linear regime). From a theoretical point of view, the previous model (1.1) should be able to describe this complex flow where both small- and large-scale structures develop. But up to our knowledge, it has never been performed with multi-dimensional compressible numerical simulations.

The aims of this paper are firstly to derive a simplified model of Hele–Shaw type (1.4) from the previous one using ideas of Ref. 27 (cf. also Refs. 2, 25 and 26), and secondly to show the feasibility of a numerical simulation of the *ablation Rayleigh–Taylor* instabilities based on this simpler model. Denoting  $\theta = T^n$ , the last equation of (1.1) leads to

$$\mathbf{u} = \theta^{1/n} \nabla \theta + \mathbf{u}_{\text{vort}}, \tag{1.2}$$

where  $\mathbf{u}_{\text{vort}}$  is the vorticity part of the velocity. If one neglects this vorticity part, then the first equation in (1.1) leads to an nonlinear diffusion equation

$$\frac{\partial}{\partial t} \left( \frac{1}{\theta^{1/n}} \right) + \Delta \theta = 0, \quad x \in \Omega. \tag{1.3}$$

The boundary conditions are very important to get the correct physical context. For Eq. (1.3) they are as follows: the simulation domain  $\Omega$  is bounded by an inner boundary  $\Gamma_c$  and an external one  $\Gamma_e$  described in Fig. 1; a nonhomogeneous Neumann boundary condition is imposed on  $\Gamma_e$ . On the inner part  $\Gamma_c$  one assumes that the temperature is lower than on the external region and one sets  $\theta = \theta_c$ . The ablative Hele–Shaw model is a further simplification of (1.3). It is based on the following consideration where one compares  $\theta_c$  to a characteristic value  $\theta_{\text{ref}}$  at the external part of the simulation domain. If the temperature  $\theta_c$  is very small compared to  $\theta_{\text{ref}}$  and if the initial data  $\theta^{\text{ini}}$  is equal to  $\theta_c$  in a part of  $\Omega$  adjacent to  $\Gamma_c$ , then the solution  $\theta(t)$  of (1.3) may be approximated by the solution  $\Theta(t)$  of the following Hele–Shaw problem (1.4):

$$\begin{cases} \Delta \Theta = 0, & x \in \Omega(t) \subset \Omega, \\ \Theta = 0, & x \in \text{on the internal moving boundary } \Gamma_f(t). \end{cases} \tag{1.4}$$

Here  $\Gamma_f(t)$  is a free boundary which moves with the time: its velocity depends on the normal derivative of  $\Theta$  (cf. Eq. (2.9)). Notice that our problem is posed in an external domain (between  $\Gamma_f$  and  $\Gamma_e$ ) even though the classical Hele–Shaw equation<sup>13</sup> is posed in an inner one. For the ablative Hele–Shaw model (1.4), the front is the curve  $\Gamma_f(t)$ . Our numerical simulations show that this approximation allows to perform numerical solution without accounting the details of the compressible fluid dynamics. This is a

major improvement in terms of simplicity of the numerical treatment. The price to pay is to use a specific numerical method on domain with moving boundaries. Here, we use the fat boundary method (FBM)<sup>4,14,15,23</sup> with a modification suggested by Maury<sup>22</sup>; it is well adapted to our problem where the deformation of the boundary is important and has to be accurately described (see Sec. 4.1.1).

The outline of this paper is as follows. In Sec. 2 starting from the previous quasi-isobar Euler system, we show how the thermo-diffusive part of this model may be approximated by a Hele–Shaw model.<sup>16</sup> Moreover we prove in a one-dimensional framework that this approximation is justified from a mathematical point of view; this fact is related to the modeling made by Kull and Anisimov.<sup>17</sup> In Sec. 3 we introduce afresh the vorticity part of the velocity and we make its coupling with the Hele–Shaw equation; so we obtain the full ablative Hele–Shaw system. Then we describe a numerical method issued from the FBM<sup>23</sup> and further developed in Refs. 4, 14 and 15 to deal with the Hele–Shaw equation. Moreover, we show the feasibility on some basic test problems. We also present numerical simulations for more complex implosion test problems with feedback of the vorticity part of the velocity.

## 2. From the Quasi-Isobar Model to the Hele–Shaw Model

According to (1.1), the velocity  $\mathbf{u}$  is the sum of a thermal velocity and a vortex velocity which is divergence-free, that is  $\mathbf{u} = \mathbf{u}_{\text{therm}} + \mathbf{u}_{\text{vort}}$  with

$$\mathbf{u}_{\text{therm}} = nT^n \nabla T \quad \text{and} \quad \nabla \cdot \mathbf{u}_{\text{vort}} = 0. \quad (2.1)$$

In what follows of this section one neglects the vorticity velocity  $\mathbf{u}_{\text{vort}}$ . Then, the density equation (1.1) may be recast as

$$\partial_t \frac{1}{T} + \nabla \cdot \left( \frac{1}{T} nT^n \nabla T \right) = 0,$$

that is Eq. (1.3).

Let us now denote  $\theta_{\text{ref}}$  a characteristic value of the temperature (to  $n$ th power) in the external part of the simulation domain. Lastly, notice that the ablation phenomena is very sensitive to small perturbations, that is, the ablation front propagation is unstable in nature. This is why we need to carefully describe the initial conditions. At  $t = 0$ , in the cold region, one assumes that  $\rho \approx \rho_c$  is almost constant and the temperature also  $\theta \approx \theta_c$ . Moreover, the cold temperature is much smaller than the reference temperature, that is

$$\frac{\theta_c}{\theta_{\text{ref}}} = \varepsilon \ll 1. \quad (2.2)$$

Convenient boundary conditions must be imposed on both parts  $\Gamma_c$  and  $\Gamma_e$  of the simulation domain; the normal external thermal flux is a data  $b^0$  which depends

slowly on time. Denoting

$$\nu = \frac{1}{n} \in \left[ \frac{2}{7}, \frac{2}{3} \right] \tag{2.3}$$

we have to address the equation

$$\begin{cases} \partial_t(\theta^{-\nu}) + \Delta\theta = 0, \\ \theta = \theta_c, & x \in \Gamma_c, \\ \partial_n\theta = b^0, & x \in \Gamma_e. \end{cases} \tag{2.4}$$

As usual,  $\partial_n$  denotes the normal derivative. For the sake of simplicity, we assume in what follows that  $b^0$  is constant with respect to the time.

**2.1. The Hele–Shaw model**

We now assume that (2.2) holds. Define

$$g(Y) = -Y^{-\nu} \quad \text{for } Y > 0. \tag{2.5}$$

Now it may be seen that a convenient time scaling is useful. So we perform in (2.4) the change of variables

$$t' = t\varepsilon^\nu\theta_{\text{ref}}^{1-\nu}, \quad \theta_\varepsilon(t', x) = \frac{\theta(t, x)}{\theta_{\text{ref}}}.$$

Thus, after dropping the prime in the time variable, (2.4) reads as

$$\begin{cases} \varepsilon^\nu\partial_t g(\theta_\varepsilon) - \Delta\theta_\varepsilon = 0, \\ \theta_\varepsilon = \varepsilon, & x \in \Gamma_c, \\ \partial_n\theta_\varepsilon = b, & x \in \Gamma_e, \end{cases} \tag{2.6}$$

where  $b = b^0/\theta_{\text{ref}}$ . Assume that the initial data  $\theta_\varepsilon(0)$  is greater than  $\varepsilon$ . Then, according to the classical theory of monotone operators (cf. Refs. 3, 6 and 8), we know that the problem is well posed and that the solution is also greater than  $\varepsilon$ . Thus the nonbounded function  $g(\cdot)$  may be replaced by a bounded one. For example, we may replace for convenience (2.5) by

$$g(Y) = \max(0, \varepsilon^{-\nu} - Y^{-\nu}) \quad \text{for } Y > 0. \tag{2.7}$$

The crucial conjecture that we will prove in dimension one is that when  $\varepsilon$  tends to zero, this problem may be approximated by a simpler one.

**Conjecture.** For convenient initial data  $\theta_\varepsilon(0, \cdot)$  (in dimension one, we precise in (2.19) what is a convenient initial data), the solution  $\theta_\varepsilon(t)$  of (2.6) is approximated by  $\Theta(t)$  in  $\mathcal{D}(t)$  and by 0 in the complementary of  $\mathcal{D}(t)$ . The function  $\Theta$  is solution of the Hele–Shaw equation

$$\begin{cases} \Delta\Theta = 0, & x \in \mathcal{D}(t), \\ \Theta = 0, & x \in \Gamma_f(t), \\ \partial_n\Theta = b, & x \in \Gamma_e. \end{cases} \tag{2.8}$$

The domain  $\mathcal{D}(t)$  is bounded on the one hand by the fixed external frontier  $\Gamma_e$  and on the other hand by the moving frontier  $\Gamma_f(t)$  whose displacement is described by

$$x'(t) = -\nabla\Theta(x(t)), \quad x(t) \in \Gamma_f(t). \tag{2.9}$$

This is similar to say that the velocity of a point  $x$  of the boundary is parallel to the outward normal  $\mathbf{n}$  and its value is equal to  $-\mathbf{n} \cdot \nabla\Theta(x)$ .

This conjecture is closely related to the result proven by Gil and Quiros<sup>9</sup> which is of the same type. Denoting  $G_\varepsilon(Y) = Y^\varepsilon$  for all  $Y > 0$ , they consider the problem

$$\partial_t G_\varepsilon(u_\varepsilon) - \Delta u_\varepsilon = 0$$

on a domain  $\Omega$  and they prove that when  $\varepsilon$  tends to 0 the solution  $u_\varepsilon(t)$  may be approximated by  $\Theta(t)$  which is a solution of a Hele–Shaw problem of the type of Eq. (2.8). In this framework the graph of  $G_\varepsilon$  converges to the graph of the Heaviside function  $H$ . In our case also one sees that when  $\varepsilon$  tends to 0,

$$\varepsilon^\nu g(Y) = \max(0, 1 - \varepsilon^\nu Y^{-\nu}) \rightarrow H(Y) \quad \text{for all } Y \geq 0.$$

Of course the position of the free boundary  $\Gamma_f$  at the initial time is related to the initial data of problem. Before proving the conjecture in dimension one, we have to study the Kull functions which are particular solutions of (2.6) on the whole real line.

**2.2. Kull’s functions**

Let us first define an universal function  $K$  related to this problem in the one-dimensional framework (cf. Ref. 17). It is the unique solution of the ordinary differential equation

$$K'(X) = 1 - K^{-\nu}(X), \quad X \in \mathbb{R}, \quad \text{with } K(0) = \left(\frac{1 + 2\nu}{1 + \nu}\right)^{1/\nu}. \tag{2.10}$$

It is trivial that  $K(X) > 1$  everywhere, that  $K(-\infty) = 1$  and that  $K$  is a convex function since we have

$$K'' = \nu K^{-(\nu+1)} K' = \nu(K^{-(\nu+1)} - K^{-(2\nu+1)}) > 0.$$

Since its third derivative is  $K''' = \nu(-(\nu + 1)K^{-(\nu+2)} + (2\nu + 1)K^{-(2\nu+2)})K'$ , the normalization at  $X = 0$  has been chosen such that  $K''$  reaches its maximum at  $X = 0$ .

**Lemma 1.** *There exist two constants  $C_1$  and  $\mu < 1$  (depending on the value of  $\nu$ ) such that*

$$K(X) \leq X + C_1, \quad X \geq 0, \tag{2.11}$$

$$K(X) \geq \mu X, \tag{2.12}$$

$$K(X) = X(1 + o(X)) \quad \text{for } X \rightarrow +\infty. \tag{2.13}$$

Moreover, for all  $L$ , we get

$$\varepsilon K\left(\frac{y}{\varepsilon}\right) - \max(0, y) \rightarrow 0, \quad \text{uniformly for } y \leq L. \tag{2.14}$$

**Proof.** According to the definition (2.10) we get the first bound; the bound (2.12) comes from the fact that  $K'(X) - \mu > 0$ , for  $X$  large enough. Relation (2.13) comes from

$$\partial_X[X - K(X)] \leq \frac{1}{(\mu X)^\nu}. \quad \square$$

**Definition of Kull’s functions.** By this universal function, the Kull’s functions are defined by

$$k_{\varepsilon, v, x_0}(x, t) = \varepsilon K\left(v \frac{x - x_0 + vt}{\varepsilon}\right),$$

where the parameters are the scaling parameter  $\varepsilon > 0$ , a positive velocity  $v$  and a shift parameter  $x_0 \in \mathbb{R}$ .

The interest of this family of functions relies on the fact that they are one-dimensional traveling waves solutions to (2.6), indeed we have

$$\varepsilon^\nu \partial_t k_{\varepsilon, v, x_0} = v^2 \varepsilon^\nu K'(X), \quad \partial_{xx} k_{\varepsilon, v, x_0} = v^2 \varepsilon^{-1} K''(X),$$

where  $X = v(x - x_0 + vt)/\varepsilon$ . Therefore, the function  $\tilde{\theta}$  defined by

$$\tilde{\theta}(t, x) = k_{\varepsilon, v, x_0}(t, x)$$

satisfies

$$-\varepsilon^\nu \partial_t (\tilde{\theta}^{-\nu}) - \partial_{xx} \tilde{\theta} = v^2 \varepsilon^{-1} \left[ \frac{\nu K'}{K^{1+\nu}} - K'' \right] = v^2 \varepsilon^{-1} [1 - K^{-\nu} - K']' = 0.$$

Moreover, we get the limits

$$\lim_{x \rightarrow -\infty} \tilde{\theta}(t, x) = \varepsilon, \quad \lim_{x \rightarrow +\infty} \partial_x \tilde{\theta}(t, x) = v.$$

### 2.3. The conjecture in dimension one

Our aim is now to prove the conjecture in the restricted one-dimensional framework where

$$\Omega = ]-\infty, L],$$

where  $L > 0$  is a fixed boundary, thus problem (2.6) reads as

$$\varepsilon^\nu \frac{\partial}{\partial t} g(\theta_\varepsilon) - \frac{\partial^2}{\partial x^2} \theta_\varepsilon = 0, \tag{2.15}$$

$$\partial_x \theta_\varepsilon|_{x=L} = b \quad \text{and} \quad \lim_{x \rightarrow -\infty} \theta_\varepsilon(x) = \varepsilon. \tag{2.16}$$

If  $b > 0$ , then this problem is well posed in the following functional space (see below the maximum principle):

$$\mathcal{L} = \{u = u(t, x), \text{ such that } \exists \lambda > 0 \text{ with } u \geq \lambda, \text{ and } u - \lambda \in \mathcal{C}^0(0, T; W^{2,1}(\Omega))\}.$$

Let us make a preliminary remark.

**Remark.** Notice that if the initial data  $\theta_\varepsilon(0)$  is equal to  $\varepsilon K(b(x - x_0)/\varepsilon)$ , then the Kull's function  $\tilde{\theta}_\varepsilon = k_{\varepsilon, b, x_0}$  solves Eq. (2.15) and we get

$$\tilde{\theta}_\varepsilon(t, -\infty) = \varepsilon, \quad \partial_x \tilde{\theta}_\varepsilon(t, L) = bK' \left( b \frac{L - x_0 + bt}{\varepsilon} \right).$$

Thus  $\tilde{\theta}_\varepsilon$  does not satisfy the right boundary condition in  $x = L$ , but if  $\varepsilon \rightarrow 0$ , we have  $\partial_x \tilde{\theta}_\varepsilon(L) \rightarrow b$ . We now define the function  $\Theta$  by

$$\Theta = \max(0, b(x - x_0 + bt)). \tag{2.17}$$

Then, for all  $t$ , we get according to (2.14)

$$\|\tilde{\theta}_\varepsilon(t, \cdot) - \Theta(t, \cdot)\|_{L^\infty(0, +\infty)} \rightarrow 0. \tag{2.18}$$

One checks that  $\Theta$  satisfies

$$\begin{cases} \partial_{xx} \Theta = 0, & x_f(t) < x < L, \\ \Theta(x_f(t), t) = 0, \\ \partial_x \Theta(L, t) = b, \end{cases}$$

where the front is at  $x_f(t) = x_0 - bt$ , therefore we have  $\partial_t(x_f(t)) = -b$ , which is equivalent to (2.9).

The previous remark leads to assume that the initial data  $\theta_{\text{ini}}$  of the system (2.15)–(2.16) has to be close to a Kull's function, more precisely it must satisfy

$$\varepsilon K \left( b \frac{x - x_0}{\varepsilon} - by \right) \leq \theta_{\text{ini}}(x) \leq \varepsilon K \left( b \frac{x - x_0}{\varepsilon} \right). \tag{2.19}$$

for two constants  $x_0 < L$  and  $y > 0$ . We now state the result corresponding to the conjecture in dimension one.

**Theorem 2.** Assume that (2.19) holds. Let  $\theta_\varepsilon$  be the solution of system (2.15)–(2.16) with initial data equal to  $\theta_{\text{ini}}$ ; then, if  $\varepsilon$  tends to 0, one has, for all  $t$ ,

$$\|\theta_\varepsilon(t) - \Theta(t)\|_{L^\infty(\Omega)} \rightarrow 0. \tag{2.20}$$

Before the proof of this result, let us give two technical lemmas and define the following distances: for all functions  $u, v$  belonging to  $\mathcal{L}$ , set

$$d(u, v) = \int_{\Omega} |g(u) - g(v)| dx \quad \text{possibly infinite,}$$

$$d^+(u, v) = \int_{\Omega} \max(0, g(u) - g(v)) dx \quad \text{possibly infinite.}$$

**Lemma 3.** *Let  $u$  and  $v$  be two functions of  $\mathcal{L}$  satisfying (2.15). Define  $u_0 = u|_{t=0}$  and  $v_0 = v|_{t=0}$ . Assume that  $\partial_x u(L, t) \leq \partial_x v(L, t)$  for all time  $t \geq 0$ . Then*

$$d^+(u(t), v(t)) \leq d^+(u_0, v_0). \tag{2.21}$$

*Assume that  $\partial_x u(L, t) = \partial_x v(L, t)$  for all time  $t \geq 0$  and that  $d(u_0, v_0)$  is finite. Then*

$$d(u(t), v(t)) \leq d(u_0, v_0). \tag{2.22}$$

**Proof.** The proof is standard in the context of nonlinear parabolic equation, except for the boundary conditions. Here,  $\varepsilon$  is of course a fixed parameter. Let us consider  $H_\eta \in C^0$  a regularization of the Heaviside function  $H$

$$H_\eta(x) = \begin{cases} 0, & x \leq -\frac{\eta}{2}, \\ \frac{x}{\eta}, & -\frac{\eta}{2} \leq x \leq \frac{\eta}{2}, \\ 1, & \frac{\eta}{2} \geq x. \end{cases}$$

Then

$$\begin{aligned} \varepsilon^\nu \int_\Omega H_\eta(u - v) \partial_t(g(u) - g(v)) dx &= \int_\Omega H_\eta(u - v) \partial_{xx}(u - v) dx \\ &= - \int_\Omega H'_\eta(u - v) |\nabla(u - v)|^2 dx \\ &\quad + H_\eta(u(L) - v(L)) \partial_x(u(L) - v(L)) \leq 0. \end{aligned}$$

Therefore

$$\int_\Omega \partial_t(H_\eta(u - v)g(u) - g(v)) dx \leq \int_\Omega (g(u) - g(v)) \partial_t(H_\eta(u - v)) dx$$

and integrating over the time interval  $[0, t]$  we get

$$\begin{aligned} \int (H_\eta(u - v)(g(u) - g(v)))(t) dx &\leq \int H_\eta(u_0 - v_0)(g(u_0) - g(v_0)) dx \\ &\quad + \int \int (g(u) - g(v)) H'_\eta(u - v) \partial_t(u - v) dx dt. \end{aligned}$$

Since  $\nu \partial_t(u - v) = -\varepsilon^{-\nu}(u^{\nu+1} \partial_{xx} u - v^{\nu+1} \partial_{xx} v)$ , it is bounded in  $L^1$ . Moreover  $(g(u) - g(v)) H'_\eta(u - v)$  is bounded in  $L^\infty$  uniformly with respect to  $\eta$ ; indeed  $g$  being Lipschitz continuous, the function  $(g(u) - g(v))/(u - v)$  is bounded. Therefore, since  $z H'_\eta(z) \rightarrow 0$  for almost all  $z$  as  $\eta \rightarrow 0$ , the dominated convergence theorem states that

$$\int_0^t \int_\Omega [(g(u) - g(v)) H'_\eta(u - v)] \partial_t(u - v) dx dt \rightarrow 0 \quad \text{for } \eta \rightarrow 0.$$

Finally

$$\lim_{\eta} \left( \int_{\Omega} (H_{\eta}(u - v)(g(u) - g(v)))(t) dx \right) = d^+(u, v)$$

is a decreasing function. It proves (2.21).

Assume now that  $d(u_0, v_0)$  is finite, that is  $\lim_{x \rightarrow -\infty} u(x) = \lim_{x \rightarrow -\infty} v(x)$  and that  $\partial_x u(L, t) = \partial_x v(L, t)$ . Then  $d^+(u, v) \leq d^+(u, v)$  and  $d^+(v, u) \leq d^+(v, u)$  which proves (2.22).  $\square$

**Lemma 4.** *Let  $u, v \in \mathcal{L}$  satisfying Eq. (2.15). Assume that  $\partial_x u(L, t) \leq \partial_x v(L, t)$  for all time  $t \geq 0$  and that  $u(0, \cdot) \leq v(0, \cdot)$ . Then we get*

$$u(t, \cdot) \leq v(t, \cdot) \quad \text{for all } 0 < t. \tag{2.23}$$

**Proof.** Notice that  $d^+(u_0, v_0) = 0$ . So the result comes from the previous lemma.  $\square$

**Proof of Theorem 2.** We may assume for the sake of simplicity that  $x_0 = 0$ . Consider the first Kull's function

$$k_1(t, x) = k_{\varepsilon, b, \varepsilon y}(t, x),$$

thus  $k_1$  satisfies  $\partial_x k_1(t, L) < b$  for all  $t$ . Moreover define  $k_2$  by

$$k_2(t, x) = k_{\varepsilon, v_{\varepsilon}, 0}(t, x)$$

such that  $\partial_x k_2(t, L) = b$ . That is  $v_{\varepsilon}$  satisfies

$$b = v_{\varepsilon} K' \left( v_{\varepsilon} \frac{L}{\varepsilon} \right) = v_{\varepsilon} - v_{\varepsilon} \left( K \left( v_{\varepsilon} \frac{L}{\varepsilon} \right) \right)^{-\nu}.$$

(It has a unique solution since  $X \mapsto XK'(X)$  is an increasing function). According to (2.12), we have  $v_{\varepsilon} \leq m_{\varepsilon}$  which solves

$$b = m_{\varepsilon} - \eta m_{\varepsilon}^{1-\nu}, \quad \text{where } \eta = \left( \frac{\mu}{L} \varepsilon \right)^{\nu}.$$

One may easily check that for  $\varepsilon$  small enough the solution  $m_{\varepsilon}$  of this equation satisfies  $m_{\varepsilon} \leq b + 2\eta b^{1-\nu}$ , thus we see that

$$b \leq v_{\varepsilon} \leq b + 2b^{1-\nu} \left( \frac{\mu}{L} \varepsilon \right)^{\nu} \varepsilon^{\nu}. \tag{2.24}$$

One has  $\theta_{\text{ini}} \leq \varepsilon K(b \frac{\cdot}{\varepsilon}) \leq k_2(0, \cdot)$ . Thus, since

$$k_1(0, \cdot) \leq \theta_{\varepsilon}(0, \cdot) \leq k_2(0, \cdot),$$

we may apply the maximum principle of Lemma 4:

$$k_1(t, \cdot) \leq \theta_{\varepsilon}(t, \cdot) \leq k_2(t, \cdot), \quad \text{for all } t > 0. \tag{2.25}$$

Therefore

$$\|\theta_{\varepsilon} - \Theta\|_{L^{\infty}(\Omega)} \leq \|\Theta - k_1\|_{L^{\infty}(\Omega)} + \|k_1 - k_2\|_{L^{\infty}(\Omega)}.$$

Since  $K' < 1$ , one checks that there exists a constant  $C$  (depending only on  $L$ ) such that for all  $\alpha$  real and  $y \leq L$ , one has

$$\varepsilon \left| K\left(\frac{\alpha + wy}{\varepsilon}\right) - K\left(\frac{\alpha + Wy}{\varepsilon}\right) \right| \leq C \max(\varepsilon, |w - W|), \quad \forall w, W > 0.$$

According to (2.24), for  $\varepsilon$  small enough, we have  $v_\varepsilon \leq V$  for a fixed  $V$ ; then we see that

$$\begin{aligned} \|k_1 - k_2\|_{L^\infty(\Omega)} &\leq \max_{x \leq L} \varepsilon \left| K\left(b \frac{x + bt}{\varepsilon}\right) - K\left(b \frac{x + v_\varepsilon t}{\varepsilon}\right) \right| \\ &\quad + \max_{x \leq L} \varepsilon \left| K\left(b \frac{x + v_\varepsilon t}{\varepsilon}\right) - K\left(v_\varepsilon \frac{x + v_\varepsilon t}{\varepsilon}\right) \right| + \varepsilon v y \\ &\leq 2c(L + Vt) \max(\varepsilon, |b - v_\varepsilon|) + \varepsilon v y = O(\varepsilon^\nu). \end{aligned}$$

Moreover, as for (2.18), one sees that, for all  $t$ ,

$$\|k_1(t, \cdot) - \Theta(t, \cdot)\|_{L^\infty(\Omega)} \leq o(\varepsilon). \tag{2.26}$$

□

### 3. The Vorticity Equation and Further Simplifications

This section deals with the vorticity part of the model (1.1). Inserting the decomposition (1.2) in the density equation  $\partial_t \rho + \mathbf{u} \cdot \nabla \rho + \rho \nabla \cdot \mathbf{u} = 0$ , we obtain the equation  $\partial_t \theta^{-\nu} + \mathbf{u}_{\text{vort}} \cdot \nabla \theta^\nu + \Delta \theta = 0$ . The complete system writes

$$\begin{cases} \partial_t \theta^{-\nu} + \mathbf{u}_{\text{vort}} \cdot \nabla \theta^\nu + \Delta \theta = 0, \\ \partial_t \mathbf{u} + \mathbf{u} \cdot \nabla \mathbf{u} + \theta^\nu \nabla P = \mathbf{g}, \\ \mathbf{u} = \theta^\nu \nabla \theta + \mathbf{u}_{\text{vort}}, \\ \nabla \cdot \mathbf{u}_{\text{vort}} = 0. \end{cases} \tag{3.1}$$

The sources of this system are the acceleration  $\mathbf{g}$  and the thermal flux at the external boundary. The system has four independent unknowns  $\theta$ ,  $\mathbf{u}$ ,  $P$  and  $\mathbf{u}_{\text{vort}}$ . The pressure  $P$  may be understood as the Lagrange multiplier associated to the free divergence constraint  $\nabla \cdot \mathbf{u}_{\text{vort}} = 0$ .

The principle of the method is to solve an advection equation for the quantity curl  $\mathbf{u}$  and couple it with the equation for the displacement of the front which has been addressed in the previous section.

#### 3.1. Accounting for the vorticity part of the velocity

According to the physics of shell implosion, the vorticity is created around the ablation front and then convected outward by the ablated material. We propose here an asymptotic model where the source terms of vorticity are located on the ablation front  $\Gamma_f$ .

Depending on the physical dimensions of the problem, it is possible to simplify further the velocity equation. From now on, our concern is on two-dimensional problems. Since we are in  $\mathbb{R}^2$ , we introduce the scalar vorticity

$$\omega = \nabla \wedge \mathbf{u} = \partial_{x_1} u_2 - \partial_{x_2} u_1.$$

Moreover, we can state the following evolution equation

$$\nabla \wedge \left( \frac{1}{T} (\partial_t \mathbf{u} + \mathbf{u} \cdot \nabla \mathbf{u}) \right) = \nabla \wedge \frac{\mathbf{g}}{T}.$$

That is an evolution equation for the vorticity

$$\partial_t \mathcal{V} + \nabla \cdot (\mathbf{u}_{\text{therm}} \mathcal{V}) = S_1 + S_2 + S_3, \quad \mathcal{V} = \frac{\omega}{T}, \tag{3.2}$$

with

$$S_1 = \nabla \wedge \frac{\mathbf{g}}{T},$$

$$S_2 = \left( \nabla \wedge \frac{1}{T} \right) (\partial_t u) - \left( \partial_t \frac{1}{T} \right) (\nabla \wedge u) = \left( \nabla \wedge \frac{1}{T} \right) (\partial_t u) - \omega \partial_t \frac{1}{T}$$

and

$$S_3 = -\nabla \cdot (\mathbf{u}_{\text{vort}} \mathcal{V}) - \nabla \wedge \left( \frac{1}{T} \nabla \frac{|u|^2}{2} \right) = -\nabla \cdot (\mathbf{u}_{\text{vort}} \mathcal{V}) - \nabla^\perp \frac{1}{T} \cdot \nabla \frac{|u|^2}{2}.$$

The effect of the acceleration  $\mathbf{g}$  is only in  $S_1$ . It is possible to simplify further the model using  $S_2 \approx S_3 \approx 0$  in order to study the influence of the acceleration only. The natural boundary condition for the advection Eq. (3.2) is on  $\Gamma_c$  where the ablation material velocity  $\mathbf{u}_{\text{therm}}$  is entering the domain. We have the Dirichlet condition  $\mathcal{V}|_{\Gamma_c} = 0$ .

There exist also simplified forms for  $S_1$ . We detail just one of them that comes from Ref. 7. The physical idea is that the support of the vorticity source terms is located around the ablation front. In this case one can perform a boundary layer analysis to estimate the source. Let us consider local coordinates  $(q, z)$ , where  $q$  represents the distance to the front  $\Gamma_f$  and  $z$  the curvilinear coordinates along  $\Gamma_f$ . The classical Kull function  $\hat{\theta}_\varepsilon(q, z, t) = \varepsilon K(V(z, t) \frac{q}{\varepsilon})$  is a boundary layer solution of the form  $\hat{\theta}_\varepsilon = \varepsilon \hat{\theta}(\frac{q}{\varepsilon}, z, t)$ , solution of  $\varepsilon^\nu \partial_t g(\theta_\varepsilon) - \Delta \theta_\varepsilon = 0$ . The approximate source term is then given by the distribution limit  $S_1 \approx \delta_{\gamma(t)} \lim_{\varepsilon \rightarrow 0} \int_{-\infty, +\infty} S_1(\hat{\theta}_\varepsilon) \chi dq$  that is at the limit

$$S_1 = (\mathbf{g} \cdot \mathbf{n}^\perp|_{\Gamma_f}) \delta_{\Gamma_f(t)}. \tag{3.3}$$

Our final simulations will use this particular form of the source term. Using the same kind of analysis, it is possible to propose also an approximation of the other source terms. It has been showed in Ref. 7 that

$$S_2 + S_3 = -(\nu \log(\alpha V) + \alpha^\nu V^\nu) \partial_z V^2 \delta_{\Gamma_f(t)} \tag{3.4}$$

is a relevant approximation localized on the front  $\Gamma_f(t)$ . Here  $V = \partial_n \Theta > 0$  and  $\nu = 1/n$ . The variable  $z$  denotes the curvilinear abscissa along the front  $\Gamma_f(t)$  and  $\alpha > 0$  is a constant with little influence since  $\nu$  is small. In the limit where  $\nu$  can be considered as very small, then

$$S_2 + S_3 \approx -\partial_z V^2 \delta_{\Gamma_f(t)} \tag{3.5}$$

is relevant. We notice that  $\int_{\Gamma_f(t)} (S_2 + S_3) dz = 0$  if the front  $\Gamma_f(t)$  is a closed curve.

### 3.2. The ablative Hele–Shaw model

Once  $\mathcal{V}$  is computed with Eq. (3.8), then the turbulent part of the velocity flow is easily computed using the representation

$$\mathbf{u}_{\text{vort}} = \nabla \wedge \varphi, \quad \varphi \in \mathbb{R}.$$

The potential  $\varphi$  satisfies the equation  $\Delta \varphi = T\mathcal{V}$  with Dirichlet boundary condition. The impact of the velocity  $\mathbf{u}_{\text{vort}}$  on the evolution of the ablation front is given by the complete thermal evolution equation

$$\varepsilon^\nu \partial_t g(\theta) + \mathbf{u}_{\text{vort}} \cdot \nabla g(\theta) - \Delta \theta_\varepsilon = 0.$$

The front  $\Gamma_f$  being considered as a thermal level set of  $\theta$ , we assume the complete evolution of the front is given by

$$\dot{x}(t) = -\nabla \Theta + \mathbf{u}_{\text{vort}}, \quad x(t) \in \Gamma_f(t).$$

Assuming this whole scenario is correct, the full ablative Hele–Shaw model reads as follows:

$$\begin{cases} -\Delta \Theta = 0, & x \in \Omega_{\text{hot}}, \\ \partial_n \Theta = v, & x \in \Gamma_e, \\ \Theta = 0, & x \in \Gamma_f, \end{cases} \tag{3.6}$$

$$\dot{x}(t) = -\nabla \Theta + \mathbf{u}_{\text{vort}}, \quad x(t) \in \Gamma_f(t), \tag{3.7}$$

where  $\mathbf{u}_{\text{vort}} = \nabla \wedge \varphi$  is defined by  $\Delta \varphi = T\mathcal{V}$  and

$$\partial_t \mathcal{V} + \nabla \cdot (\mathbf{u}_{\text{therm}} \mathcal{V}) = S_1, \quad x \in \Omega. \tag{3.8}$$

## 4. Numerical Approximation

To our knowledge the discretization of the Hele–Shaw equation was addressed for the first time in Ref. 13. In what follows we describe a new numerical method for the calculation of approximate solutions to the Hele–Shaw problem with feedback of the vorticity. The main numerical problem encountered at the numerical level is the discretization of the Hele–Shaw problem (4.1)–(4.2) without the vorticity

$$\begin{cases} -\Delta \Theta = 0, & x \in \Omega_{\text{hot}}, \\ \partial_n \Theta = v, & x \in \Gamma_e, \\ \Theta = 0, & x \in \Gamma_f, \end{cases} \tag{4.1}$$

where the moving boundary is  $t \mapsto \Gamma_f(t)$ ,

$$\dot{x}(t) = -\nabla\Theta, \quad x(t) \in \Gamma_f(t), \tag{4.2}$$

because the boundary  $\Gamma_f$  is a moving one. So we need to use a method for the coupling of the Poisson equation (4.1) with the boundary condition on  $\Gamma_f$ . Moreover we need a correct level of accuracy: if not the displacement of the boundary might be of poor accuracy. Up to our knowledge, one of the most efficient method for this task is the FBM which has been proposed in dimension two by Maury<sup>23</sup> (see also Refs. 4, 14 and 15) [an alternative is the fictitious domain technique for which we refer the reader to Ref. 10]. The originality in our paper is the adaptation of this method to the convergent Hele–Shaw equation and the coupling with the vorticity equation. In a first part we describe the adaptation of this method to our Hele–Shaw problem and some numerical results to validate the approach. In a second part we describe the coupling with the vorticity equation using a finite volume technique.

**4.1. Discretization of the Hele–Shaw equation with the fat boundary method**

The moving boundary (4.2) at time  $t_k = k\Delta t$  is discretized with markers  $x_q^k \in \mathbb{R}^2$ . The chain of markers

$$(x_q^k)_{q=1,\dots,Q} \text{ with periodic condition}$$

is the discrete approximation of the moving boundary. In all our numerical investigations, this chain is a closed loop. At  $t_0 = 0$  the  $(x_q^0)$  are given. We now address the harmonic equation (4.1) at time step  $t_k$ . The displacement of points  $x_q^k$  will be described just afterward.

So Eq. (4.1) is discretized with the very classical finite difference method on a Cartesian grid (equivalent to a  $Q^1$  finite element method with mass lumping,<sup>5,24</sup> also equal to a  $P^1$  finite element method on a specific triangular grid)

$$-\frac{\Theta_{i+1,j} + \Theta_{i-1,j} + \Theta_{i,j+1} + \Theta_{i,j-1} - 4\Theta_{i,j}}{\Delta x^2} = 0. \tag{4.3}$$

The difficulty is that the degrees of freedom of the boundary, that is the markers  $x_q^k$ , are not on the nodes  $x_{i,j} = (i\Delta x, j\Delta x)$  of the Cartesian mesh.

The numerical coupling of these two different discretization will be insured with the FBM. Essentially the FBM allows to compute the normal derivative  $\partial_n\Theta$  with an accuracy which is sufficient to move the markers at the end of the time step. In principle any discrete method can be used, provided enough accuracy is reached for the displacement of the internal boundary. Our experience is that very good results are obtained with this method.

**4.1.1. Principle of the FBM**

We describe the principle of the method adapted to the problem with a Neumann condition. For the simplicity of the presentation we go back to the partial differential

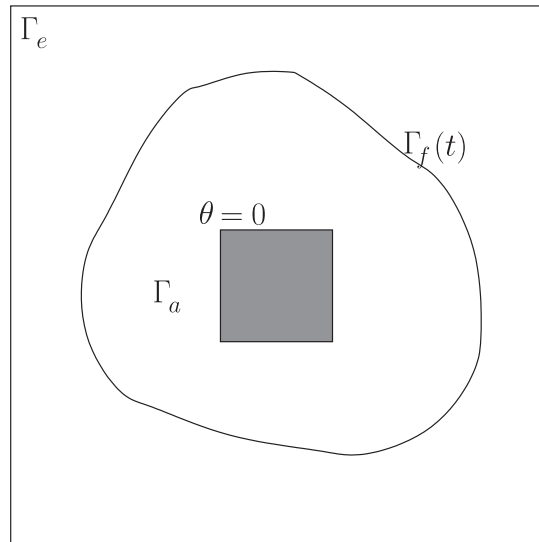


Fig. 2. Geometry of the problem described in Eq. (4.4).

formulation of the problem. Let us consider that  $\Gamma_f$  is given. In the FBM the unknown  $\Theta$  of (4.1) is extended by continuity to zero in the interior domain delimited by  $\Gamma_f$ . That is one first rewrites (4.1) as

$$\begin{cases} -\Delta\Theta = (\partial_n\Theta)\delta_{\Gamma_f}, & x \in \Omega, \\ \partial_n\Theta = v, & x \in \Gamma_e, \\ \Theta = 0, & x \in \Gamma_a, \end{cases} \tag{4.4}$$

where  $\delta_{\Gamma_f}$  is the Dirac measure on the curve  $\Gamma_f$ . The Dirichlet boundary on  $\Gamma_a$  guarantees the well posedness of the problem. The geometry of the problem is described in Fig. 2.

We replace the normal derivative by a fat boundary approximation<sup>15</sup>  $\partial_n\Theta \approx \Phi(\Theta)$  where the operator  $\Phi$  is defined by

$$\Phi(\Theta)(x) = \frac{\Theta(x + \varepsilon n(x))}{R(x) \ln(1 + \varepsilon/R(x))}, \quad x \in \Gamma_f, \tag{4.5}$$

where  $R(x)$  is the local curvature of  $\Gamma_f$ ,  $n(x)$  is the normal and  $\varepsilon$  is the size of the fat boundary. For small  $\varepsilon$  this quantity is a good estimation of the normal derivative. This method is related to the introduction of a crust domain around the boundary  $\Gamma_f$ ; it is well adapted to our problem. Notice that this formula using a well chosen value of  $\varepsilon$  as proposed by Maury<sup>22</sup> (see below) has the benefit to be simple and accurate. Indeed, the approximation (4.5) is actually an identity for the solution  $\varphi$  of a Laplace equation with radial symmetry

$$\partial_{rr}\varphi + \frac{1}{r}\partial_r\varphi = 0 \Leftrightarrow r\partial_r\varphi = k \in \mathbb{R} \Leftrightarrow \varphi = k(\log r - \log R), \quad r \geq R,$$

where the parameters are  $k$  and  $R > 0$ , the constant curvature of the boundary on which the homogeneous Dirichlet condition is imposed. For such a solution one

checks that

$$\Phi(\varphi(R)) = \partial_n \varphi(R)$$

is the exact Dirichlet to Neumann operator. In the case of a boundary with a non-constant curvature, the procedure (4.5) incorporates an additional numerical error in the algorithm but is a way to simplify the initial FBM.<sup>23</sup> All our numerical tests show that the method is accurate. So we obtain the system

$$\begin{cases} -\Delta\Theta = V\delta_{\Gamma_f}, & x \in \Omega, \\ \partial_n\Theta = v, & x \in \Gamma_e, \\ \Theta = 0, & x \in \Gamma_a, \\ V = \Phi(\Theta), & x \in \Gamma_f. \end{cases} \tag{4.6}$$

This system is solved by the iteration procedure  $p \rightarrow \infty$

$$\begin{cases} -\Delta\Theta^{p+2} = V^{p+1}\delta_{\Gamma_f}, & x \in \Omega, \\ \partial_n\Theta^{p+2} = v, & x \in \Gamma_e, \\ \Theta^{p+2} = 0, & x \in \Gamma_a, \\ V^{p+1} = \kappa V^p + (1 - \kappa)\Phi(\Theta^p), & x \in \Gamma_f. \end{cases} \tag{4.7}$$

At each iteration of this procedure, one has to assemble the right-hand side  $V^{k+1}\delta_{\Gamma_f}$ : this is done with standard numerical integration techniques. The algorithm is controlled by two parameters  $\kappa$  and  $\varepsilon$ .

- The parameter  $\varepsilon$  measures the quality of the approximation of the Neumann data. So small  $\varepsilon$  are required for accuracy, but not too small so that the evaluation of the Neumann data is accurate on a grid with characteristic length  $\Delta x$ . This alternative is visible in Ref. 15 where two different prescriptions of  $\varepsilon$  are proposed: one is  $\varepsilon \approx \Delta x^2$  and is not possible in our case; the other one is  $\varepsilon$  proportional to a typical length of the problem. In our calculations  $\varepsilon$  is in the order of the cell size and we take  $\varepsilon \approx 3\Delta x$ . We observed that it is sufficient to get an accurate numerical approximation on a Cartesian grid, at least the accuracy is sufficient for our purposes. We refer to Fig. 3 for a detailed explanation of the numerical construction of the operator (4.5): this is easily done because an accurate definition of the radius of curvature of the normal is possible without difficulty from the knowledge of the markers which define  $\Gamma_f$ .
- The parameter  $0 < \kappa < 1$  is a regularization parameter. For the initial FBM,<sup>23</sup> it has been demonstrated that an optimal value exists to guarantee the convergence of the algorithm. The algorithm we use in this paper is slightly different but the spirit of the method is the same. In practice, we observed that the rate of convergence depends of course on the value of parameter  $\kappa$  and has to be tuned (according to the value chosen for  $\varepsilon$ ). For our computations we find a good compromise between robustness and accuracy and we take  $\kappa \approx 0.1$ .

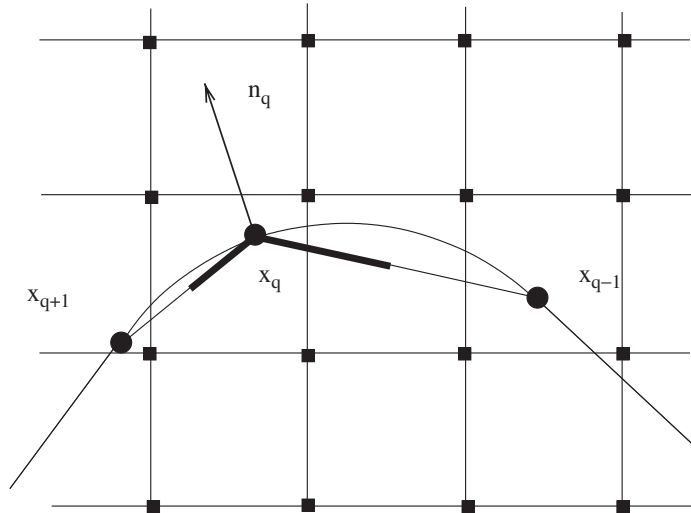


Fig. 3. Discretization on the front  $\Gamma_f$ . The length  $l_q$  is the half sum of the lengths of both sides, that is  $l_q = 1/2 d(x_{q-1}, x_q) + 1/2 d(x_q, x_{q+1})$ . The normal  $n_q$  is equal to the normal of the circle  $C_q$  such that  $x_{q-1}, x_q, x_{q+1} \in C_q$ . It guarantees a good accuracy of the calculation of the normal at the front. The squares are the degrees of freedom of the Poisson equation  $\Theta_{ij}$ .

#### 4.1.2. Practical solution of (4.1) with the FBM

We discretize the Poisson equation in (4.7) with a finite element method, using the variational formulation

$$\int \nabla \Theta^{p+2} \cdot \nabla \varphi_j \, dx = \int_{\Gamma_f} V^{p+1} \varphi_j \, d\sigma + \int_{\Gamma_e} v \varphi_j \, d\sigma.$$

Here  $\varphi_j \in X_h$  is a test function. The space of shape functions is defined by

$$X_h = \{u_h \in C^0(\Omega); u_h = 0 \text{ on } \Gamma_a; u_h|_{T_i} \in P_1(T_i)\}.$$

There is no difficulty to discretize the boundary integral  $\int_{\Gamma_e} v \varphi_j \, d\sigma$ . Concerning the integral on  $\Gamma_f$  we use the approximate formula

$$\int_{\Gamma_f} V^{p+1} \varphi_j \, d\sigma = \sum_{q=1}^Q V_q^{p+1} \varphi_j(x_q) l_q,$$

where  $x_q$  denotes markers and  $l_q$  denotes the average length of the front. The discrete value of  $\varphi_j(x_q)$  is naturally defined by interpolation. The estimation of length  $l_q$  is explained in Fig. 3, together with the normal vector  $n_q$ . The local radius of curvature  $R_q$  is defined in a consistent fashion.

Concerning the fourth equation of (4.7), the important feature is the discretization of the function  $\Phi$  at the markers position. We use the approximation<sup>14,15,23</sup>

$$\Phi(\Theta^p(x_q)) = \frac{\Theta^p(x_q + \varepsilon n_q)}{R_q \ln(1 + \frac{\varepsilon}{R_q})},$$

where  $\Theta^p(x_q + \varepsilon n_q)$  is obtained by  $Q^1$  interpolation from the grid values  $\Theta_{i,j}^p$ .

So the discretization of each step of the iteration procedure (4.7) is well defined. In practice we iterate  $p$  until practical convergence is reached. With this method we are able to solve the Poisson equation in function of the markers at all time steps  $t_k$ . It defines a map

$$\Gamma^k = (x_q^k)_{1 \leq q \leq Q} \mapsto \Theta = \Theta^{(k)}.$$

4.1.3. Displacement of the markers with Eq. (4.2)

This is the easy part of the algorithm. We use the first-order explicit Euler approximation

$$\frac{x_q^{k+1} - x_q^k}{\Delta t} = \Phi(\Theta(x_q^k)), \tag{4.8}$$

where  $\Phi(\Theta(x_q^k))$  has been defined previously.

4.1.4. The Hele–Shaw problem with radial solution

Proofs of convergence for the FBM are technical and restricted to very particular cases.<sup>15,23</sup> Instead we rely on specific test cases to evaluate the accuracy of the method and to validate our choices.

In this first test case the external Neumann condition is modified such that

$$\Theta(r, t) = vR_c \log \left( \frac{r}{\sqrt{r_0^2 - 2vR_c t}} \right)$$

is an analytic solution. At a certain time a numerical solution is plotted in Fig. 4. The evolution in time of the radius of  $\Gamma_{\text{int}}$  is compared with the analytic law  $r = \sqrt{r_0^2 - 2vR_c t}$  in Fig. 5. The comparison is excellent and in favor of the use of the FBM for the numerical approximation of the Hele–Shaw equation.

Next we increase the number of points to evaluate the stability and accuracy of the method, see Fig. 5. The data are the same. It shows a correct behavior of the overall algorithm.

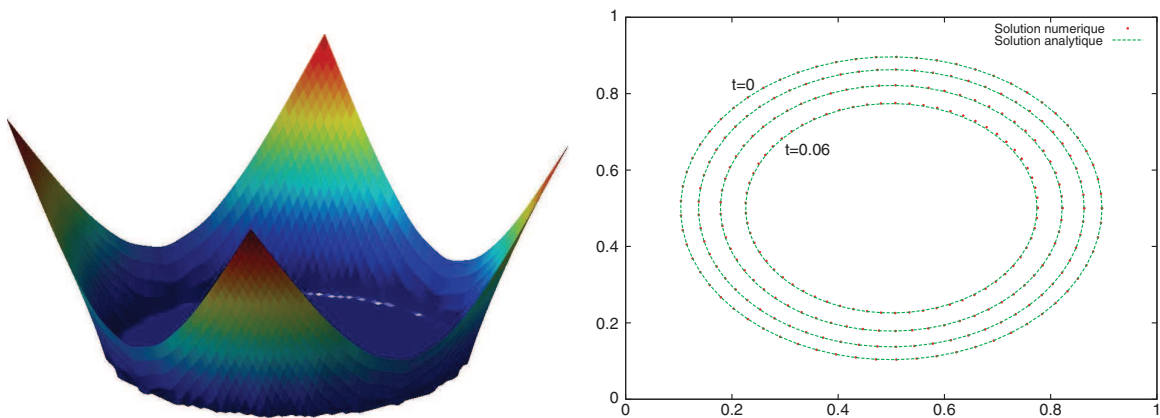


Fig. 4. On the left:  $\Theta = T^k$  at a certain time step. On the right: the markers at three different times. Computed with 65 markers on a grid  $65 \times 65$ .



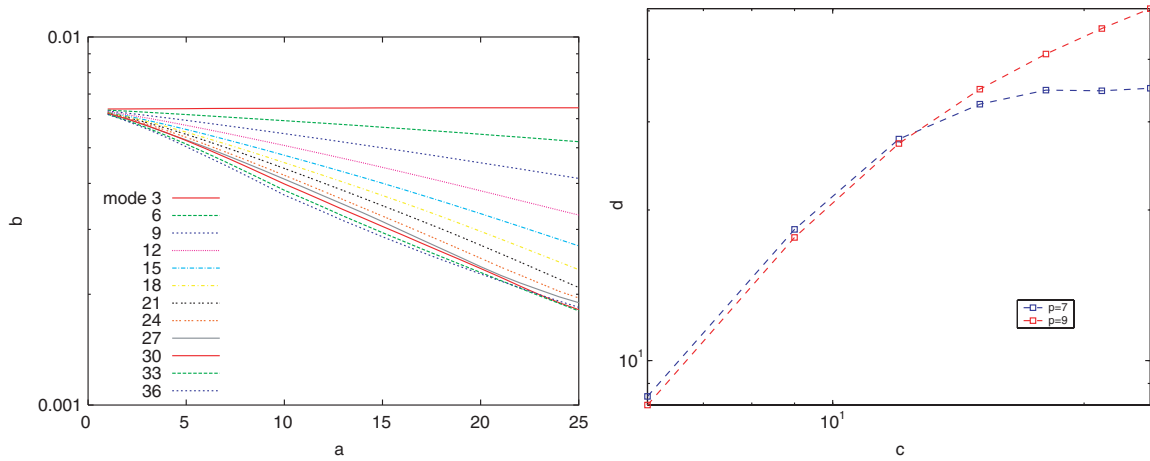


Fig. 7. On the left: evolution in time of the amplitude of modes,  $t \mapsto a_l(t)$ , log-scaled. On the right: dispersion relation for  $18 > l > 3$ . We used to spatial relations of the form  $h = \frac{1}{2^{l+1}}$ .

Denoting  $a_l(t)$  the amplitude of the perturbation at time  $t$ , we check from the numerical experiments as it is predicted by the theory that one has  $a_l(t) \approx \exp(-\sigma(l)t)$ . A typical result is depicted in Fig. 7, where we plot the evolution in time of the amplitude of the perturbations (log-scaled). The stabilizing or smoothing effect is more pronounced for higher modes. This is compatible with the linear theory. We also plot the graph of the dispersion relation, which gives  $\sigma(l)$  as a function of  $18 > l > 3$ . These results are qualitatively in good accordance with the results of Masse.<sup>21</sup> More precisely  $\sigma(l) \approx c_1 l^2$  for low  $l$ . On the other hand  $\sigma(l) \approx c_2 l$  for higher modes  $l > 15$ . Once again this is compatible with Masse’s results. The effect of the numerical diffusion is difficult to evaluate.

**4.2. Coupling with the vorticity equation**

To deal numerically with the full system (3.6)–(3.8), the strategy is the following. At each time step  $t_k$ ,

- (i) we solve Eq. (3.6) with given markers  $x_q^k$ ,
- (ii) we solve the advection Eq. (3.8) with a finite volume technique to get  $\mathcal{V}$  and by a standard technique  $\mathbf{u}_{\text{vort}}$  which is related to the solution  $\varphi$  of equation  $\Delta\varphi = \omega$ ,
- (iii) we move the markers with velocity  $\mathbf{u}_{\text{therm}} + \mathbf{u}_{\text{vort}}$  (as described above).

We focus on the numerical method to solve Eq. (3.8).

**4.2.1. Discretization of the vorticity equation (3.8)**

It is based on a classical finite volume scheme.<sup>11</sup> We have observed that a first-order approximation gives poor results, as it is often the case for convection-dominated problems. So we have to use a second-order technique for the solution of the vorticity

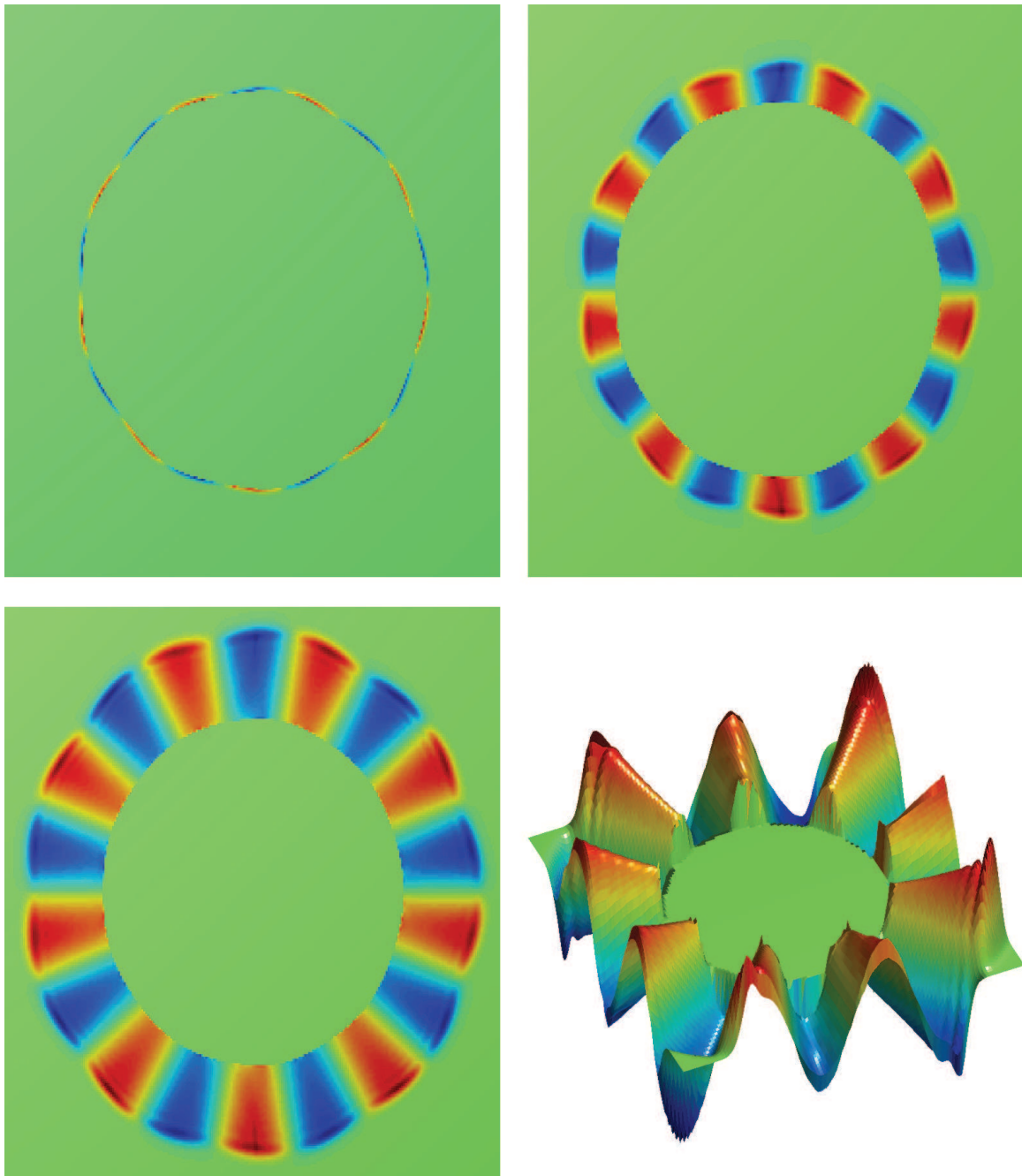


Fig. 8. The initial data is a front  $\Gamma_f$  discretize with 100 markers and with a mode 9. We plot the vorticity at three different times. Bottom figures correspond to the same physical time.

equation coupled with the Hele–Shaw equation. In our case it is based on the standard second-order MUSCL procedure.<sup>18,29</sup>

More precisely, we define the degrees of freedom on the nodes of the Cartesian mesh already used to discretize the Hele–Shaw problem. That is, we consider the scheme

$$\Delta x \frac{\mathcal{V}_{i,j}^{k+1} - \mathcal{V}_{i,j}^k}{\Delta t} + \mathbf{u}_{i+\frac{1}{2},j}^{\text{therm}} \mathcal{V}_{i+\frac{1}{2},j}^{\star} - \mathbf{u}_{i-\frac{1}{2},j}^{\text{therm}} \mathcal{V}_{i-\frac{1}{2},j}^{\star} + \mathbf{u}_{i,j+\frac{1}{2}}^{\text{therm}} \mathcal{V}_{i,j+\frac{1}{2}}^{\star} - \mathbf{u}_{i,j-\frac{1}{2}}^{\text{therm}} \mathcal{V}_{i,j-\frac{1}{2}}^{\star} = S_{i,j}, \tag{4.9}$$

where  $\mathbf{u}_{i,j}^{\text{therm}}$  is the thermal velocity at the boundaries of the square centered around the node  $(i, j)$ ,  $\mathcal{V}_{i,j}^{\star}$  is the flux density and  $S_{i,j}$  is the source term of the equation.

The thermal velocity which is a gradient is naturally discretized. One has the natural approximation

$$\mathbf{u}_{i+\frac{1}{2},j}^{\text{therm}} = \frac{n}{n+1} \frac{(\Theta_{i+1,j}^k)^{\frac{n+1}{n}} - (\Theta_{i,j}^k)^{\frac{n+1}{n}}}{\Delta x}.$$

Similar formulas hold on the other interfaces  $(i - \frac{1}{2}, j)$ ,  $(i, j + \frac{1}{2})$  and  $(i, j - \frac{1}{2})$ .

The flux density  $\mathcal{V}_{i+\frac{1}{2},j}^{\star}$  is evaluated explicitly by the standard minmod limiter which reads, with  $\mu = \delta t / \delta x$ ,

if  $\mathbf{u}_{i+\frac{1}{2},j}^{\text{therm}} > 0$ ,

$$\text{then } \mathcal{V}_{i+\frac{1}{2},j}^{\star} = \mathcal{V}_{i,j}^k + \frac{1}{2} (1 - \mu \mathbf{u}_{i+\frac{1}{2},j}^{\text{therm}}) \min\text{mod}(\mathcal{V}_{i+1,j}^k - \mathcal{V}_{i,j}^k, \mathcal{V}_{i,j}^k - \mathcal{V}_{i-1,j}^k)$$

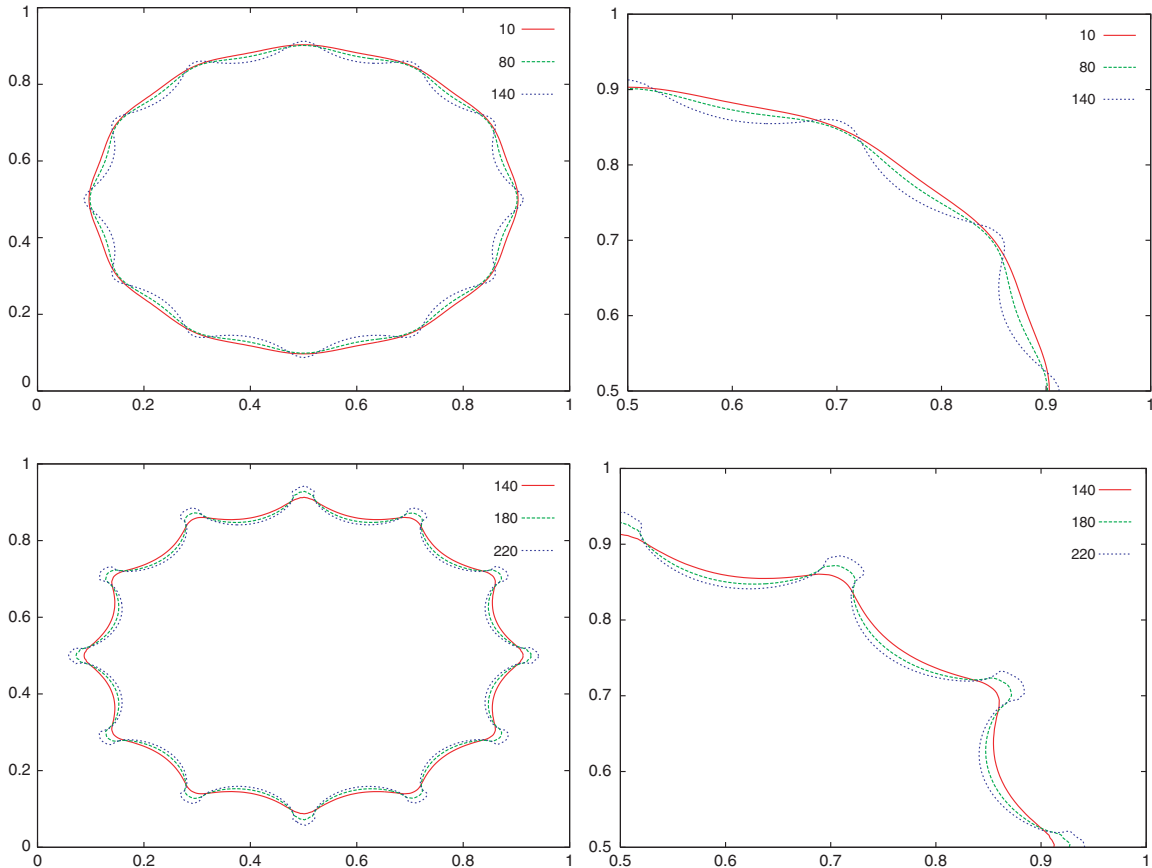


Fig. 9. The ablation front at five different times (top:  $t = 10, 80$  and  $140$ , bottom:  $t = 140, 180$  and  $220$ ). The gravity is  $g = 1000$ . At  $t = 0$  the front is discretized with 100 markers with a mode 12. The results show first the development of an instability first in a linear regime, and then in a nonlinear regime.

and

$$\text{if } \mathbf{u}_{i+\frac{1}{2},j}^{\text{therm}} \leq 0,$$

$$\text{then } \mathcal{V}_{i+\frac{1}{2},j}^{\star} = \mathcal{V}_{i+1,j}^k + \frac{1}{2}(1 - \mu \mathbf{u}_{i+\frac{1}{2},j}^{\text{therm}}) \text{minmod}(\mathcal{V}_{i,j}^k - \mathcal{V}_{i+1,j}^k, \mathcal{V}_{i+1,j}^k - \mathcal{V}_{i+2,j}^k).$$

The minmod function is given by  $\text{minmod} = \frac{1}{2}(\text{sgn}(a) + \text{sgn}(b)) \min(|a|, |b|)$ .

#### 4.2.2. Some numerical results

We first do not introduce the action of the vorticity in the markers (4.8). It means that the vorticity is computed in a passive way and has no influence on the Hele–Shaw problem. A typical result is plotted in Fig. 8. We see that vorticity is generated at the front. The front is a convergent one. The vorticity is going outward with velocity  $\mathbf{u}^{\text{therm}}$ .

Moreover, we address the full problem with the coupling of the vorticity on the moving boundary. The nonzero source term  $S_1$  is given in formula (3.3) with an acceleration  $|\mathbf{g}| = 1000$ . A typical result is displayed in Fig. 9 where the vorticity part

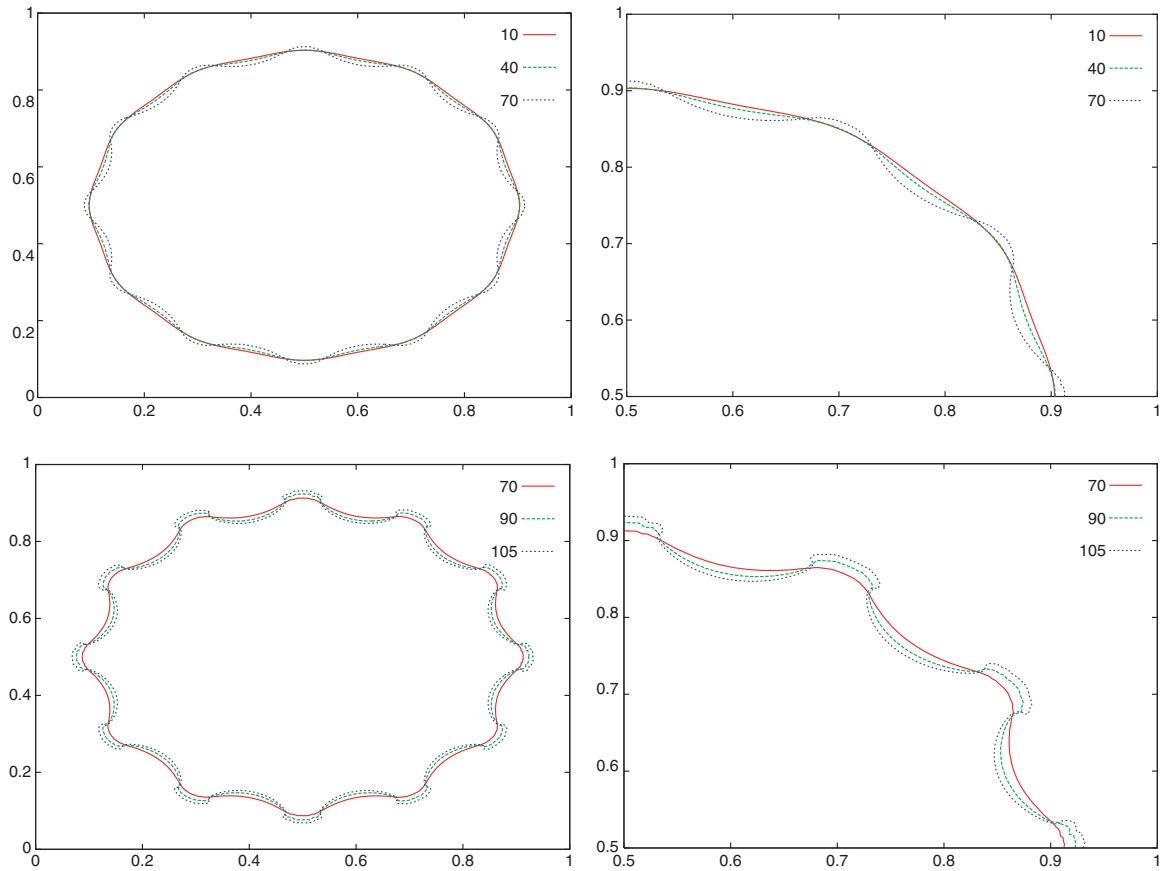


Fig. 10. The ablation front at five different times (top:  $t = 10, 40$  and  $70$ , bottom:  $t = 70, 90$  and  $105$ ). The gravity is  $g = 5000$ . At  $t = 0$  the front is discretized with 100 markers with a mode 12. The results show first the development of an instability first in a linear regime, and then in a nonlinear regime. The dynamics is slightly more pronounced than with a lower acceleration (cf. Fig. 9).

of the velocity field is computed using  $S_2 = S_3 = 0$ . It shows that the backward coupling of the vorticity is such that the growth of the instability of the ablation front is important.

In Fig. 10 we have performed a similar simulation with the same initial parameters as for the simulation displayed in Fig. 9, but the acceleration is multiplied by a factor 5:  $|\mathbf{g}| = 5000$ . We observe a similar behavior, but the dynamics is more pronounced, in particular one sees the development of large bubbles earlier; this is in agreement with the physical interpretation of this phenomenon.

Our last simulations are made with the source term  $S_2 + S_3$  (see Eq. (3.4)). This term is easy to discretize because the tangential derivative  $\partial_z \cdot$  has a natural and evident definition as shown in Fig. 3. Some results are displayed in Figs. 11 ( $|\mathbf{g}| = 200$ ) and 12 ( $|\mathbf{g}| = 5000$ ). We observe the same global behavior of the instability development as in

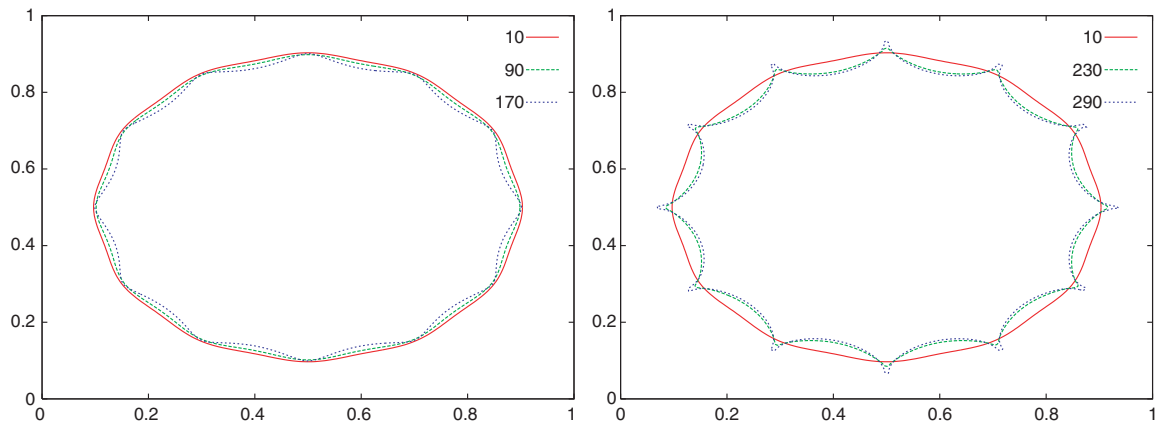


Fig. 11. The ablation front at five different times:  $t = 10, 90, 170, 230$  and  $290$ , the source term is  $S_1 + S_2 + S_3$  with  $g = 200$ . At  $t = 0$  the front is discretized with 100 markers with a mode 12. The results show first the development of an instability first in a linear regime, and then a strong development in a nonlinear regime. By comparison with the previous results, an important difference is the presence of cusps which are therefore associated with the source term  $S_2 + S_3$ .

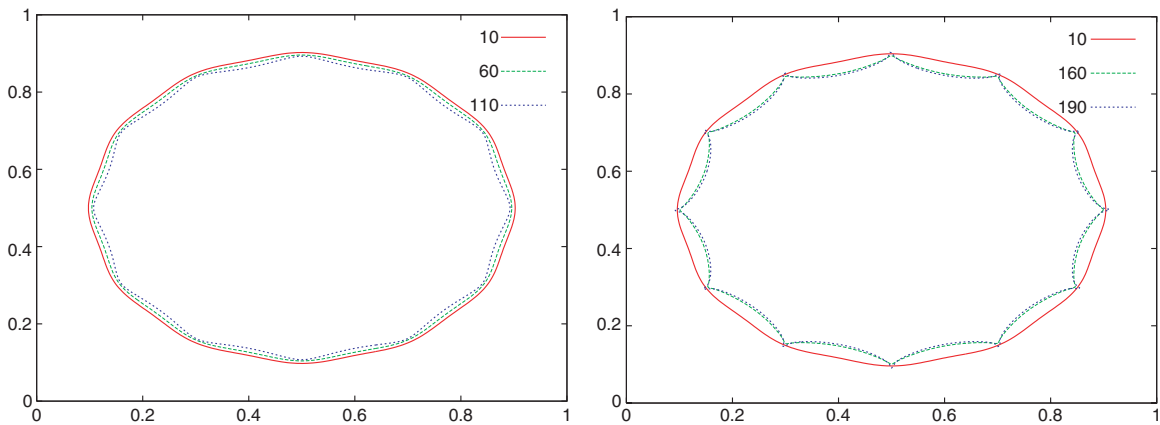


Fig. 12. The ablation front at five different times:  $t = 10, 60, 110, 160$  and  $190$ . The gravity is  $g = 0$  that is the source term is  $S_2 + S_3$ . At  $t = 0$  the front is discretized with 100 markers with a mode 12. It confirms that the cusps are due to the tangential derivative in  $S_2 + S_3$ .

previous simulation with only  $S_1$  but one sees that the occurring of so-called cusps instead of bubbles.

### 5. Conclusion

We have proposed a simplification of the quasi-isobar compressible model in the context of the simulation of the ablative Rayleigh–Taylor instabilities. The model is a Hele–Shaw type equation supplemented by additional terms for the vorticity part of the velocity field. We have explained that numerical methods are efficient for the discretization of these equations on a Cartesian grid in a two-dimensional framework. In our case, we used a special version<sup>15</sup> of the FBM.<sup>4,14,23</sup>

We have observed in the numerical results that the ablation front is stabilized by the thermal conduction part of the model. But of course the vorticity part of the velocity field may be a germ of instability. Depending on the nature of the coupling, the instability may be smooth (mushrooms) or less smooth (cups).

These preliminary numerical results show the feasibility of a numerical method based on the proposed Hele–Shaw model.

### Appendix A. Justification of the Quasi-Isobar Model

The starting point is the compressible Euler model

$$\begin{cases} \partial_t \rho + \nabla \cdot (\rho \mathbf{u}) = 0, \\ \partial_t \rho \mathbf{u} + \nabla \cdot (\rho \mathbf{u} \otimes \mathbf{u}) + \nabla p = 0, \\ \partial_t (\rho e) + \nabla \cdot (\rho \mathbf{u} e + p \mathbf{u}) - \nabla \cdot (\kappa n T^n \nabla T) = 0, \end{cases} \tag{A.1}$$

written in the domain  $\Omega$  described in Fig. 1, corresponding to a spherical shell. The total energy  $e$  is given by  $e = \mathcal{E} + \frac{1}{2}|\mathbf{u}|^2$ , where  $\mathcal{E}$  is the internal energy;  $T$  denotes the temperature and  $p = (\gamma - 1)\rho\mathcal{E} = \rho T$  the pressure; so  $\mathcal{E} = C_v T$ . The two first equations are related to the evolution of the density  $\rho$  and the velocity  $\mathbf{u}$ , the third one is the total energy balance with a nonlinear heat flux, it reads also

$$\partial_t(\rho\mathcal{E}) + \nabla \cdot (\rho\mathbf{u}\mathcal{E}) + p\nabla \cdot \mathbf{u} - \nabla \cdot (\kappa n T^n \nabla T) = 0.$$

The energy equation has to be supplemented by a boundary condition on the external boundary  $\Gamma_e$  which is a nonhomogeneous Neumann condition (related to the heating of the spherical shell by a thermal flux) and by a Dirichlet condition on the inner boundary  $\Gamma_c$ . On the external boundary  $\Gamma_e$ , since the velocity is outward, there is no boundary condition for the equations of the density and momentum. The boundary conditions for these equations on the inner boundary  $\Gamma_c$  are addressed below.

#### A.1. Change of referential

We make some remarks that are at the basis of the modeling.

**Remark A.1.** In the experiments we have in mind, the material is initially cold and dense and is ablated by the thermal flux at a surface denoted by  $\Gamma_f(t)$  called “ablation

front”; this surface is moving and propagates inward. In the neighborhood of  $\Gamma_f$ , the density varies with a sharp gradient from the cold region where  $\rho \simeq \rho_c$  (with  $\rho_c$  constant) to the hot region where  $\rho \ll \rho_c$ ; and there the temperature varies from  $T \simeq T_c$  to the hot level  $T \gg T_c$ . This is represented in Fig. A.2 which is a cut along the radial direction. The subscript  $\cdot_c$  refers to the cold region.

**Remark A.2.** As shown in Fig. 1, it may be assumed that the geometry is locally planar, at least for the sake of simplicity to perform the following change of referential. One must account for the fact that a first shock have traveled through the ablative matter and a reflective shock travels from the inner boundary  $\Gamma_c$  toward the external one. Then the ablative matter is driven with a macroscopic velocity  $\mathbf{u}_{\text{macro}}$ ; this velocity has a direction normal to the boundaries  $\Gamma_c$ , which is oriented inward and its modulus is a given function which is assumed to depend smoothly on the time variable. We will now state the system in the referential, which moves with this velocity and we define  $x'$  by

$$x' = x - \int_0^t \mathbf{u}_{\text{macro}}(\tau) d\tau.$$

Now denoting by the primes ( $\cdot'$ ) the quantities evaluated in the moving referential

$$\mathbf{u}'(t, x') = \mathbf{u}(t, x) - \mathbf{u}_{\text{macro}}, \quad \rho'(t, x') = \rho(t, x), \quad T'(t, x') = T(t, x).$$

One gets after well-known manipulations

$$\begin{cases} \partial_t \rho' + \nabla' \cdot (\rho' \mathbf{u}') = 0, \\ \partial_t \rho' \mathbf{u}' + \nabla' \cdot (\rho' \mathbf{u}' \otimes \mathbf{u}') + \nabla' p' = \rho' \mathbf{g}, \\ \partial_t (\rho' \mathcal{E}') + \nabla' \cdot (\rho' \mathbf{u}' \mathcal{E}') + p' \nabla' \cdot \mathbf{u}' - \nabla' \cdot (\kappa n T'^n \nabla T') = 0, \end{cases} \tag{A.2}$$

where we have introduced the acceleration  $\mathbf{g} = \frac{\partial}{\partial t} \mathbf{u}_{\text{macro}}$ .

**A.2. The quasi-isobar model**

Since the material speed is assumed to be small compared to the speed of sound, we may now perform a low Mach number approximation. Recall that the pressure is proportional to the product of the density and the temperature. Heuristically, the low Mach number approximation may be viewed as follows; see Ref. 1 or Ref. 12 for a more rigorous analysis.

Dropping the primes and using the Lagrangian derivative  $D_t = \partial_t + \mathbf{u} \cdot \nabla$ , system (A.2) reads as

$$\begin{cases} D_t \rho + \rho \nabla \cdot \mathbf{u} = 0, \\ \rho D_t \mathbf{u} + \nabla p = \rho \mathbf{g}, \\ \frac{1}{\gamma - 1} D_t p + \frac{\gamma}{\gamma - 1} p \nabla \cdot \mathbf{u} - \nabla \cdot (\kappa n T^n \nabla T) = 0. \end{cases} \tag{A.3}$$

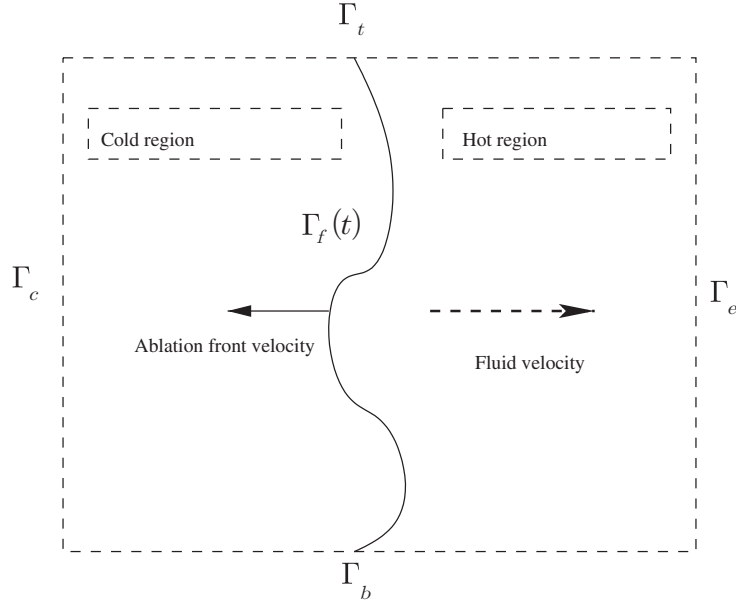


Fig. A.1. A zoom near the ablation front  $\Gamma_f$  which propagates toward the left of the domain.

Introduce now a characteristic length  $l^\star$  and characteristic values  $\rho^\star$  and  $T^\star$  of the density and of the temperature in the hot region, see Fig. A.1 and set

$$u^\star = T^{\star 1/2}, \quad t^\star = \frac{l^\star}{u^\star}, \quad p^\star = \rho^\star T^\star, \quad g^\star = \frac{T^\star}{l^\star}.$$

Then we define dimensionless variables  $\Phi_\star = \Phi/\Phi^\star$  for all variables and we obtain

$$\begin{cases} D_{t_\star} \rho_\star + \rho_\star \nabla_\star \cdot \mathbf{u}_\star = 0, \\ \rho_\star D_{t_\star} \mathbf{u}_\star + \frac{1}{M^2} \nabla_\star p_\star = \rho_\star \mathbf{g}_\star, \\ \frac{1}{\gamma - 1} D_{t_\star} p_\star + \frac{\gamma}{\gamma - 1} p_\star \nabla_\star \cdot \mathbf{u}_\star - H \nabla_\star \cdot (n T_\star^n \nabla_\star T_\star) = 0. \end{cases} \quad (\text{A.4})$$

The dimensionless numbers are

- the Mach number  $M^2 = \rho^\star |u^\star|^2 / p^\star$ ;
- $H = \kappa n (T^\star)^{n+1} / (p^\star u^\star) = \kappa n (T^\star)^{n+1} / (\rho^\star T^{\star 3/2})$  measures the velocity of the particles in the hot region.

The Froude number  $1/g_\star$  is a measure of the acceleration of the particles coming through the internal boundary  $\Gamma_c$  into the cold region.

Next we perform an asymptotic expansion of all variables with respect to the square of the Mach number

$$\begin{cases} \rho_\star = \rho_\star^{(0)} + M^2 \rho_\star^{(2)} + \dots, \\ \mathbf{u}_\star = \mathbf{u}_\star^{(0)} + M^2 \mathbf{u}_\star^{(2)} + \dots, \\ p_\star = p_\star^{(0)} + M^2 p_\star^{(2)} + \dots, \\ T_\star = T_\star^{(0)} + M^2 T_\star^{(2)} + \dots. \end{cases}$$

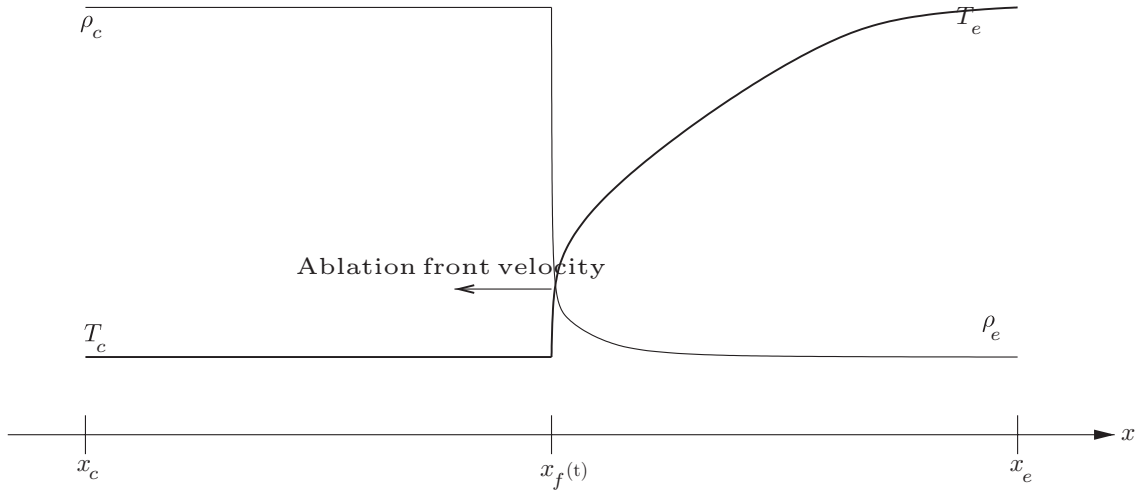


Fig. A.2. Radial cut, shape of density and thermal fields. The velocity of the front is  $\dot{\Gamma}_f(t) < 0$ .

Inserting this expansion into (A.4) one gets

$$\begin{cases} D_{t_\star} \rho_\star^{(0)} + \rho_\star^{(0)} \nabla_\star \cdot \mathbf{u}_\star^{(0)} = 0, \\ \rho_\star^{(0)} D_{t_\star} \mathbf{u}_\star^{(0)} + \nabla_\star p_\star^{(2)} = \rho_\star^{(0)} \mathbf{g}_\star, \\ \frac{1}{\gamma - 1} D_{t_\star} p_\star^{(0)} + \frac{\gamma}{\gamma - 1} p_\star^{(0)} \nabla_\star \cdot \mathbf{u}_\star^{(0)} - H \nabla_\star \cdot (n(T_\star^{(0)})^n \nabla_\star T_\star^{(0)}) = 0. \end{cases} \tag{A.5}$$

One also has  $p_\star^{(0)} = \rho_\star^{(0)} T_\star^{(0)}$  and  $\nabla p_\star^{(0)} = 0$ . Since  $\nabla p_\star^{(0)} = 0$ , the value of  $p_\star^{(0)}$  is set by the boundary condition or by any global condition that we do not want to discuss. It is therefore reasonable to assume that  $p_\star^{(0)}$  is a constant also in time. That is  $D_{t_\star} p_\star^{(0)} = 0$ . One can assume that this constant is equal to 1 without restriction. We now set

$$P = p_\star^{(2)}, \quad \rho = \rho_\star^{(0)}, \quad T = T_\star^{(0)}, \quad \mathbf{u} = \mathbf{u}_\star^{(0)}.$$

The quasi-isobar pressure law in dimensionless variable reads as  $\rho T = 1$ . We may choose  $\rho_\star$  such that  $H = \gamma/(\gamma - 1)$ , then we get the system stated in Sec. 1.

To have a schematic representation of picture of the ablative front, see Fig. A.2 where there is a cut of the map of the quantities  $\rho, T$  along the radial direction; one shows a singular surface where both the density and the temperature have very strong gradients.

### References

1. T. Alazard, Low Mach number limit of the full Navier–Stokes equations, *Arch. Rational Mech. Anal.* **180** (2006) 1–73.
2. C. Almarcha, P. Calvin, L. Duchemin and J. Sanz, Ablative Rayleigh–Taylor instability with strong temperature dependence of the thermal conductivity, *J. Fluid. Mech.* **579** (2007) 481–492.

3. P. Bénilan and S. S. De Léon, Accretivity, T-accretivity: The uniqueness-comparison theorem for strong solutions, *Semesterbericht Funktionalanalysis* (Tubingen, 1989), pp. 15–44.
4. S. Bertoluzza, M. Ismail and B. Maury, Analysis of the fully discrete fat boundary method, *Numer. Math.*, doi:10.1007/s00211-010-0317-4.
5. P. Ciarlet, *The Finite Element Method for Elliptic Problems*, Vol. 40 (SIAM, PA, 2002).
6. M. G. Crandall and T. Liggett, Generation of semi-groups of nonlinear transformations on general Banach spaces, *Amer. J. Math.* **93** (1971) 265–298.
7. H. Egly, Contribution to modelization and simulation of ablative-like Rayleigh–Taylor instabilities for ICF, Ph.D. thesis, 2007.
8. L. C. Evans, Application of nonlinear semigroup theory to certain partial differential equations, in *Nonlinear Evolution Equations* (Proc. Symp., Univ. Wisconsin, 1978), pp. 163–188.
9. O. Gil and F. Quiros, Convergence of the porous media equation to Hele–Shaw, *Nonlinear Anal.* **44** (2001) 1111–1131.
10. V. Girault and R. Glowinski, Error analysis of a fictitious domain method applied to a Dirichlet problem, *Japan J. Indust. Appl. Math.* **12** (1995) 487–514.
11. E. Godlewski and P. A. Raviart, *Numerical Approximation of Hyperbolic Systems of Conservation Laws*, Vol. 118, Applied Mathematical Sciences (Springer, 1991).
12. H. Guillard and A. Murrone, On the behavior of the upwind scheme in low Mach number limit, ii. *Comput. Fluids* **33** (2004) 655–675.
13. S. D. Howison and J. M. Aitchison, Numerical computation of Hele–Shaw flows with free boundaries, *J. Comput. Phys.* **60** (1985) 376–390.
14. M. Ismail, The fat boundary method for the numerical resolution of elliptic problems in perforated domains. Application to 3D fluid flows, Ph.D. thesis, University Paris, Orsay, 2004. Hal server, <http://tel.archives-ouvertes.fr/tel-00006401/en/>.
15. M. Ismail and B. Maury, The fat boundary method for the numerical resolution of elliptic problems in perforated domains. Application to 3D fluid flows, *Proc. du 35ème Congrès Nat. d’Ana. Num.*, 2003, pp. 1–25.
16. I. C. Kim, Regularity of the free boundary for the one phase Hele–Shaw problem, *J. Differential Equations* **223** (2005) 161–184.
17. H. J. Kull and S. I. Anisimov, Ablative stabilization in the incompressible Rayleigh–Taylor instability, *Phys. Fluids* **29** (1986) 2067–2075.
18. R. Leveque, *Finite Volume Methods for Hyperbolic Problems* (SIAM, 2002).
19. J. D. Lindl, *Inertial Confinement Fusion* (AIP, 1998).
20. P. L. Lions, *Mathematical Topics in Fluid Mechanics*, Oxford Lecture Series in Mathematics and its Applications (Oxford Univ. Press, 1998).
21. L. Masse, Etude linéaire de l’instabilité du front d’ablation en fusion par confinement inertiel, Ph.D. thesis, 2001.
22. B. Maury, private communication.
23. B. Maury, A fat boundary method for the Poisson equation in a domain with holes, *J. Sci. Comput.* **16** (2001) 319–339.
24. P. A. Raviart, *Introduction à l’analyse Numérique des Équations aux Dérivées Partielles* (Dunod, 2004).
25. J. Sanz, Self-consistent analytical model of the Rayleigh–Taylor instability in inertial confinement fusion, *Phys. Rev. Lett.* **73** (1994) 2700–2703.
26. J. Sanz, R. Betti, R. Ramis, J. Ramírez and R. P. J. Town, Nonlinear theory of the ablative Rayleigh–Taylor instability, *Phys. Rev. Lett.* **89** (2002) 195002-1–195002-4.

27. J. Sanz, A. R. Piriz and L. F. Ibanez, Rayleigh–Taylor instability of steady ablation front: The discontinuity model revised, *Phys. Plasmas* **4** (1997) 1117–1126.
28. L. Monthiery, H. Takabe, K. Mima and R. Morse, Self-consistent of the Rayleigh–Taylor instability in ablatively accelerated plasma, *Phys. Fluids* **28** (1985) 3676–3682.
29. E. Toro, *Riemann Solvers and Numerical Methods for Fluid Dynamics*, 2nd edn. (Springer, 1999).